Electronic Supplementary Material (ESI) for RSC Advances.

Supporting Information

Cancer theranosis using mono-disperse, mesoporous gold nanoparticles obtained via a robust, high-yield synthetic methodology

Taeksu Lee, Doyeon Bang, Young Wook Chang, Yuna Choi, Kwang Yeol Park, Aram Oh, Seungmin Han, Sun Hee Kim, Kwangyeol Lee, Jin-Suck Suh, Yong-Min Huh, and Seungjoo Haam**

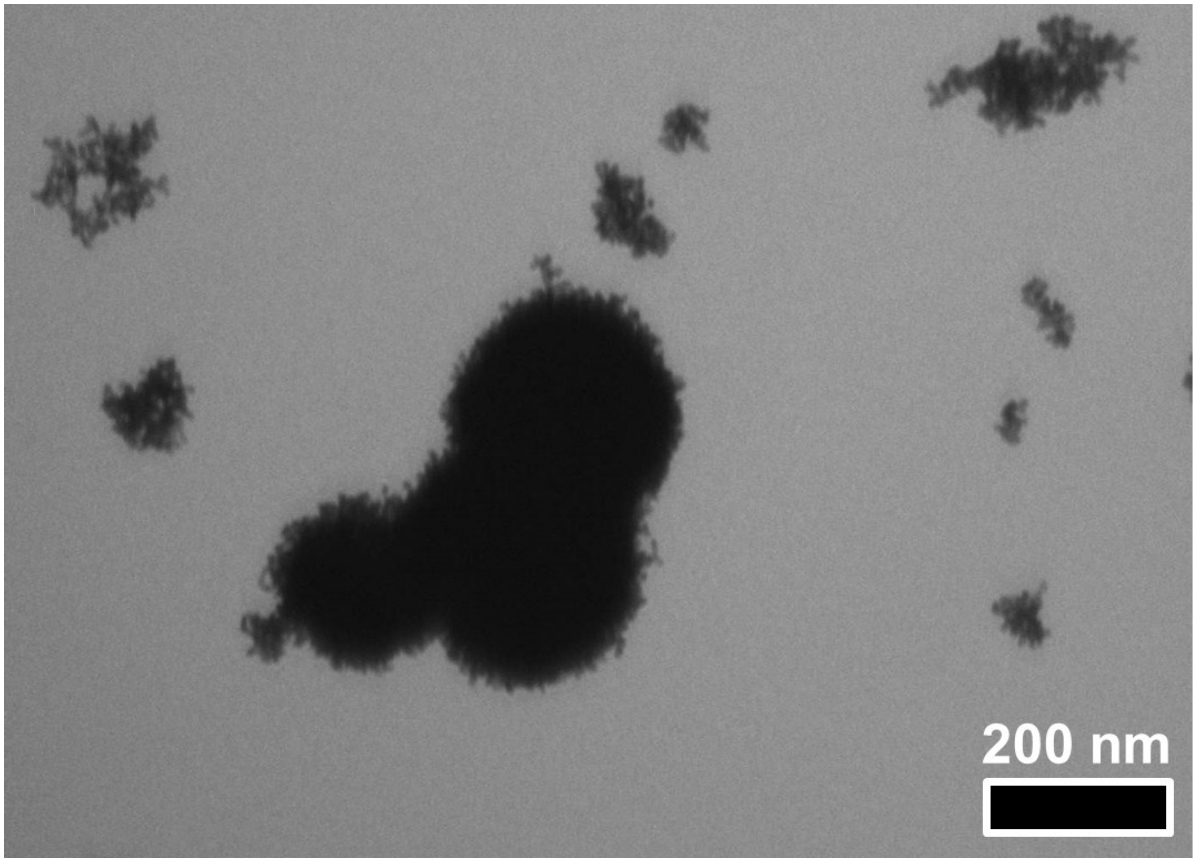

Figure S1. Representative TEM image of WNBs synthesized in a neutral aqueous solution.

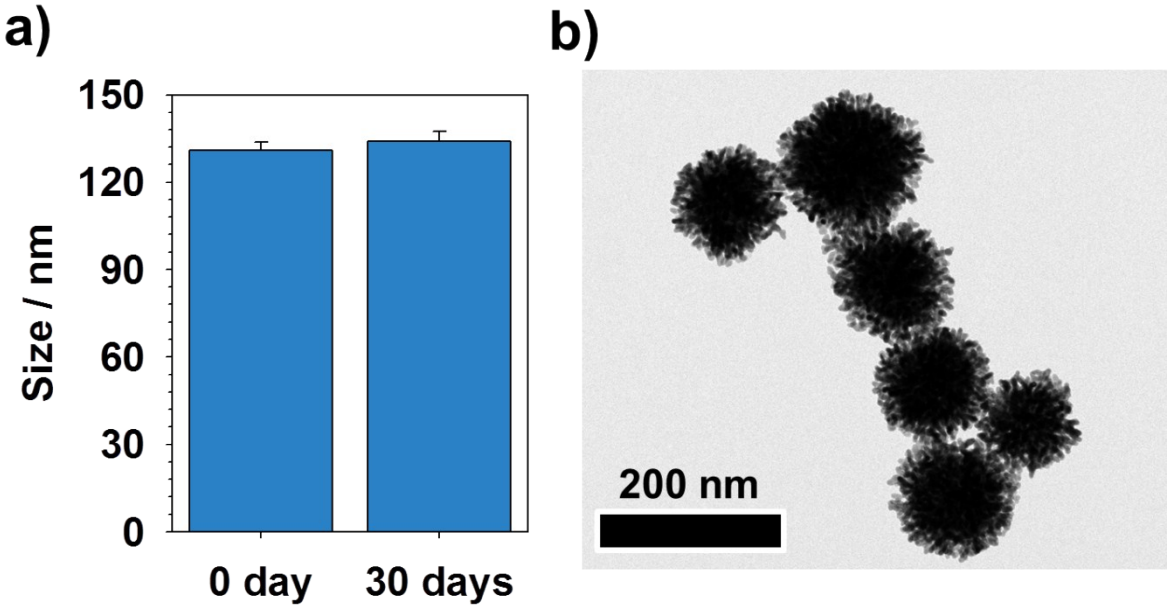

Figure S2. a) Size variation of MPGNs over 30 days and b) TEM images of MPGNs 30 days after synthesis

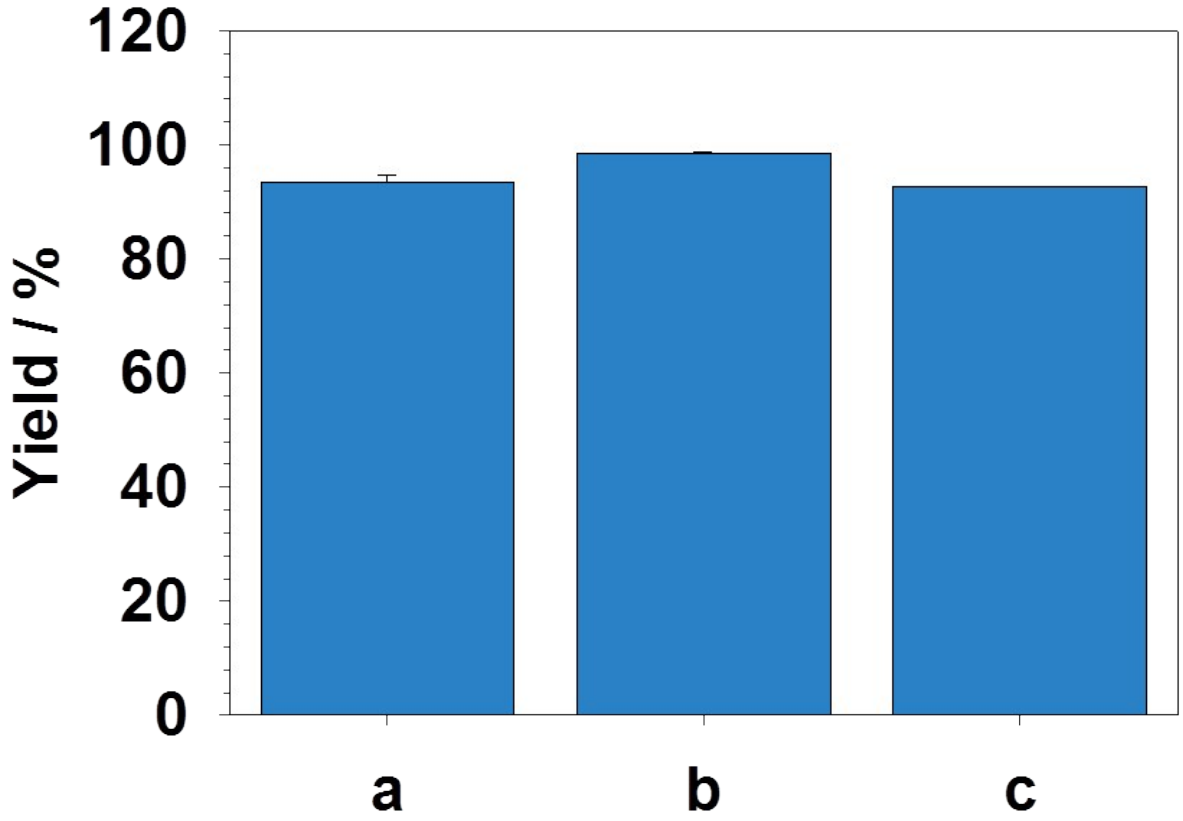

Figure S3. Relative synthetic yield of MPGNs with varying MPGN size. All yields were above 90% regardless of MPGN diameter. (a) 131.0 ± 2.7 nm; b) 309.6 ± 7.72 nm; c) 391.9 ± 12.0 nm).

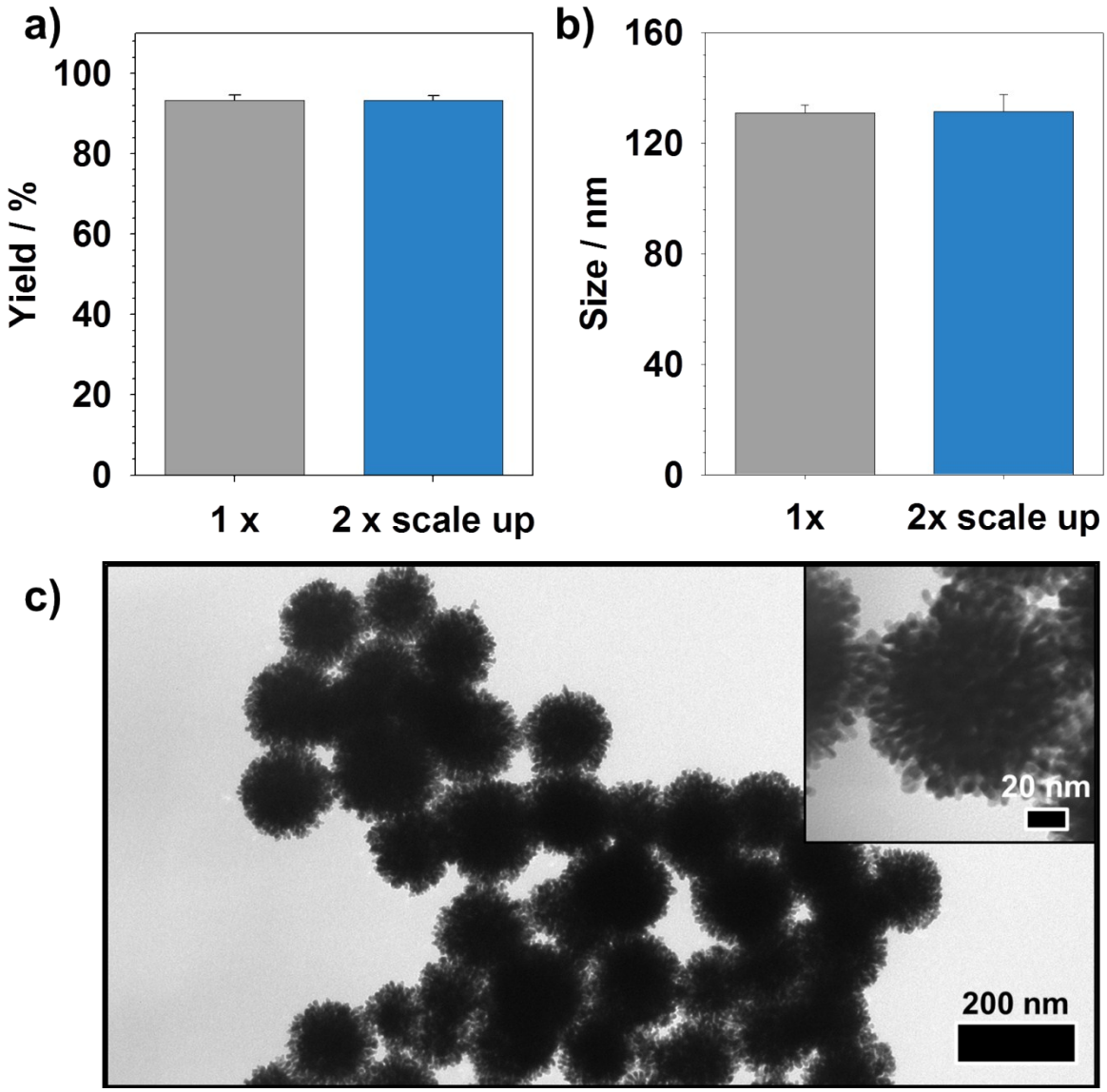

Figure S4. a) Relative synthetic yield and b) hydrodynamic diameter of MPGNs before and after 2x scale up. Synthetic yield was measured using ICP-OES, and hydrodynamic diameter was analyzed by light scattering. c) Representative TEM images of MPGNs after 2x scale up. The inset is the magnified MPGN image.

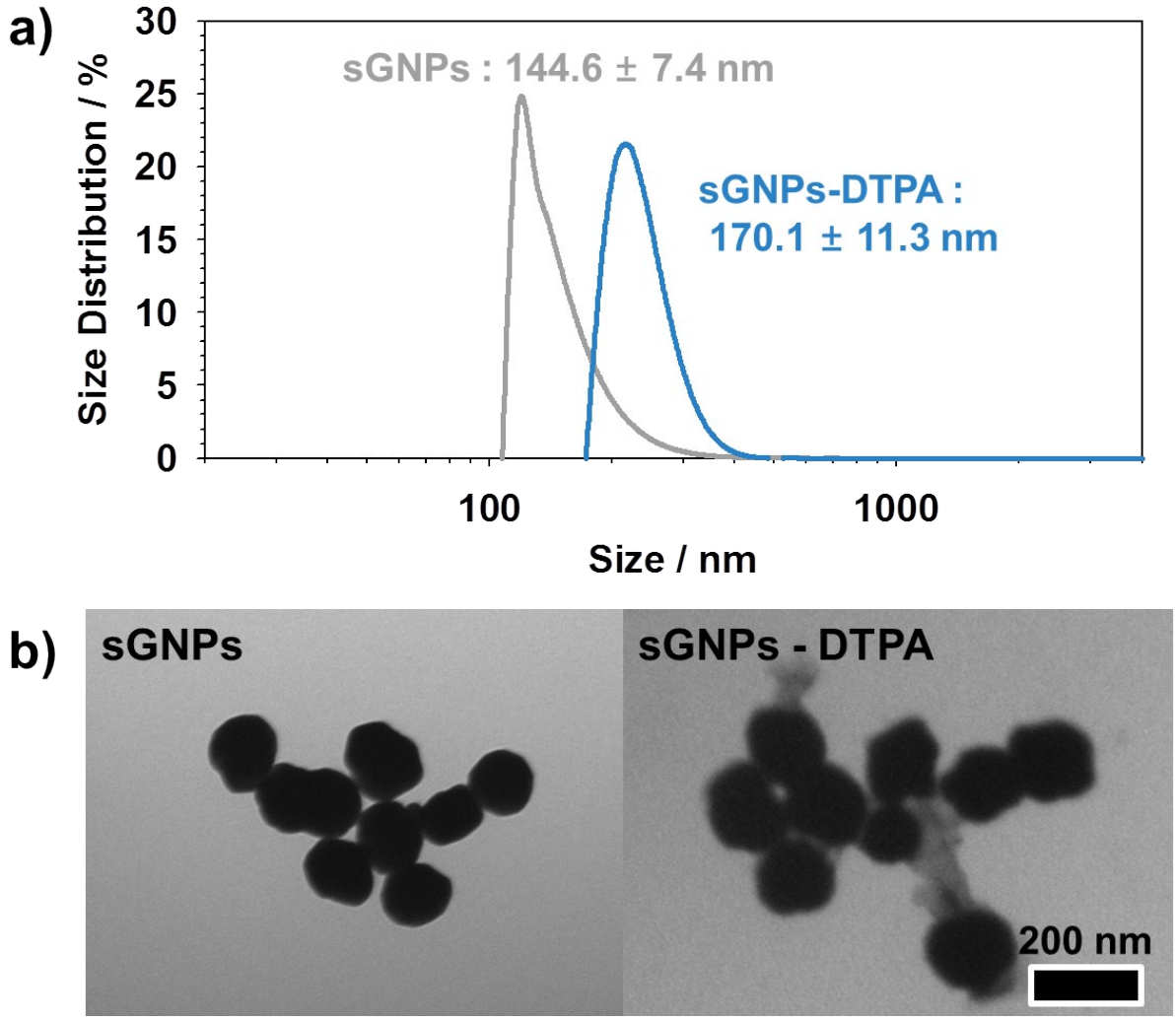

Figure S5. a) Size distribution of sGNPs and DTPA- and Gd-modified sGNPs using light scattering at room temperature. After surface modification, sGNPs size increased to 170.1 ± 11.3 nm. b) Representative TEM images of sGNPs and DTPA- and Gd-modified sGNPs.

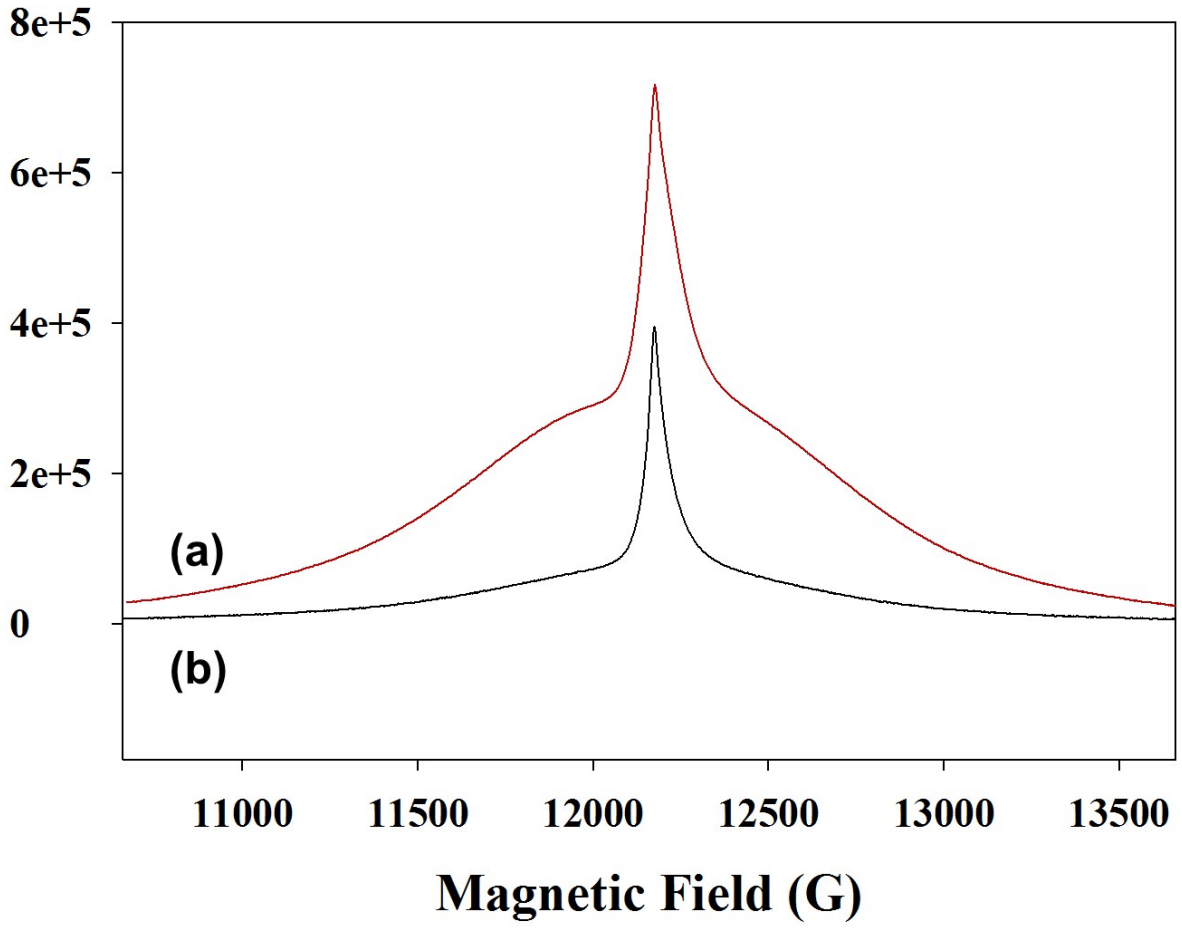

Figure S6. Three-pulse electron spin echo (ESE) field-sweep spectra of (a) $GdCl_3$ and (b) CG-MPGNs.

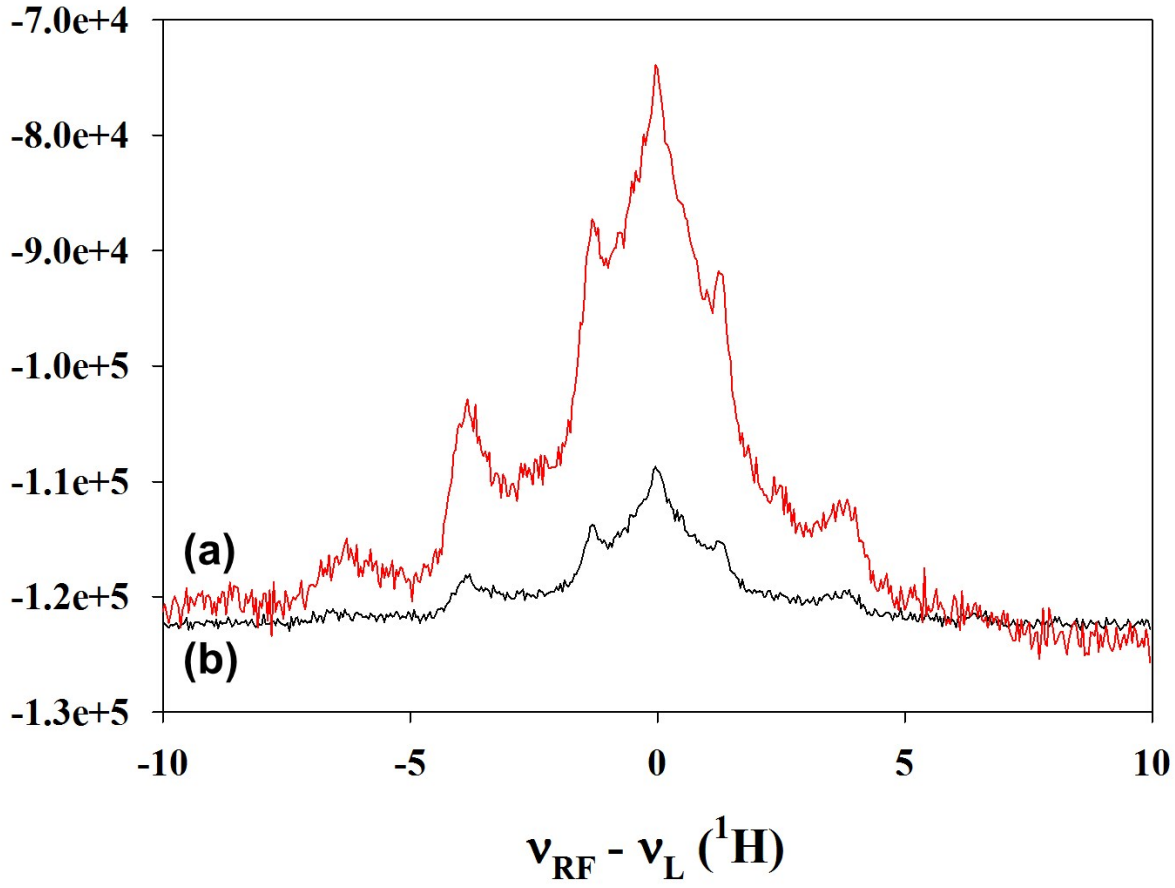

Figure S7. ^{1}H-Mims ENDOR spectra of (a) $GdCl_3$ and (b) CG-MPGNs. All spectra were taken at 8 K.

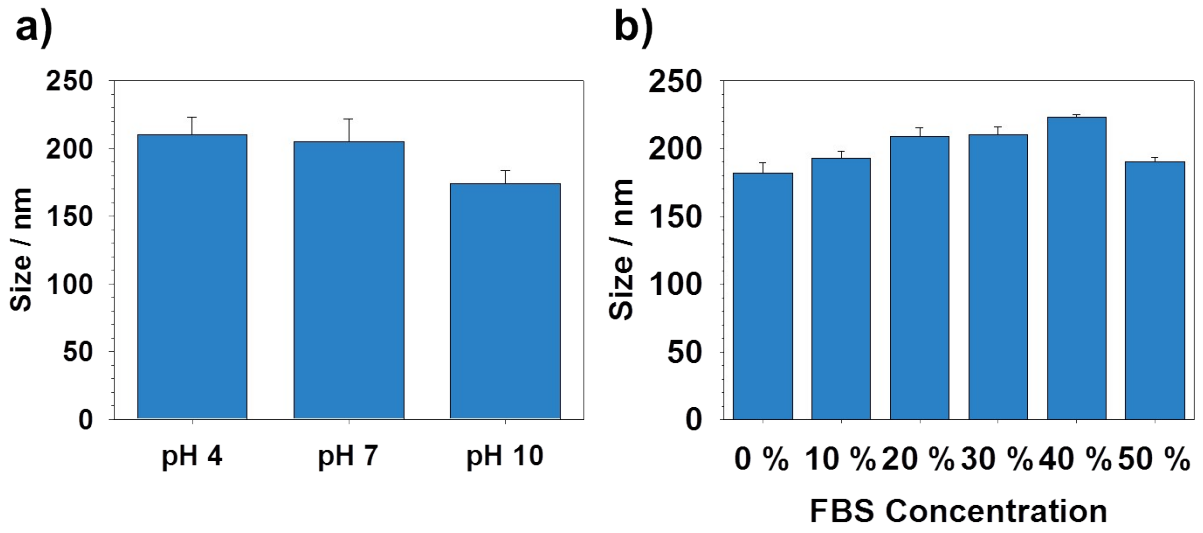

Figure S8. Size of CG-MPGNs at a) different pH conditions and b) varying fetal bovine serum (FBS) concentrations, as determined by laser scattering.

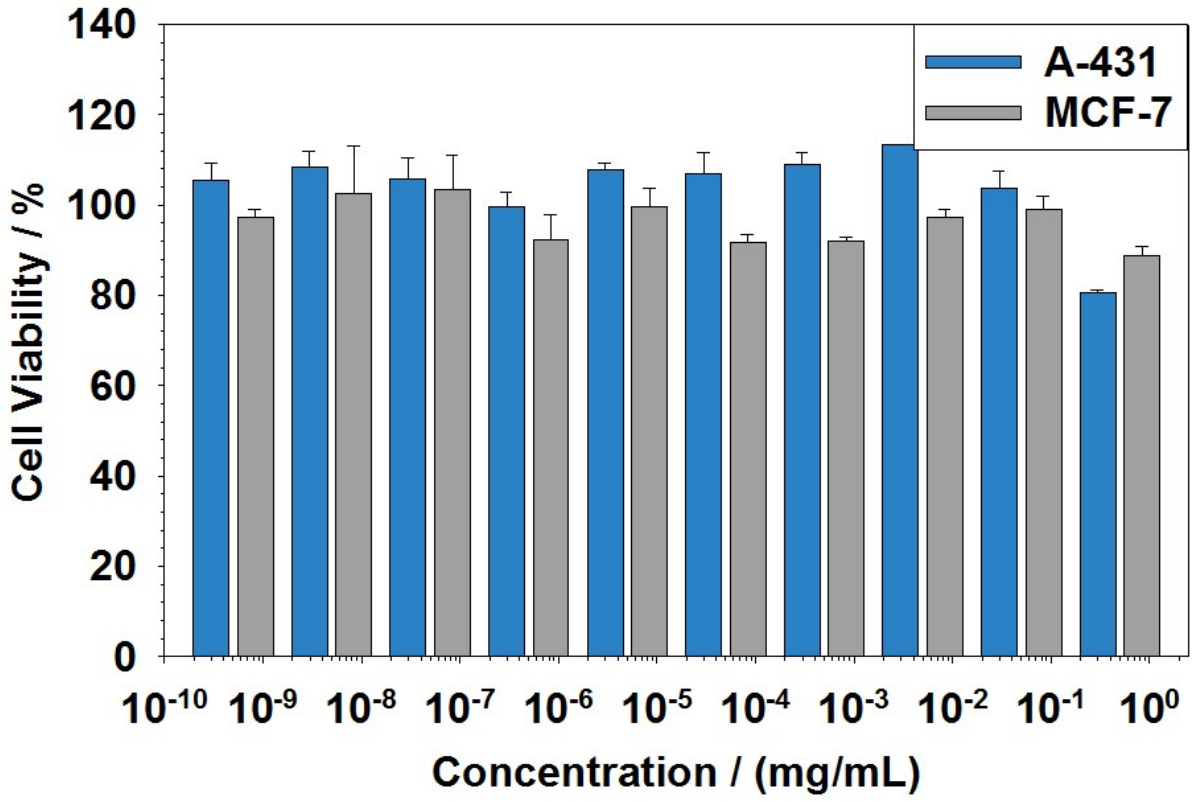

Figure S9. Cell viability test of various concentrations of CG-MPGNs (5×10^{-11} − 5×10^{-1} mg/mL) against A-431 (blue bar) and MCF-7 (gray bar) cell lines (1×10^4 cells each) using the 3-(4,5-dimethylthiazolyl-2)-2,5-diphenyltetrazolium bromide (MTT) assay at 37 °C in a 5% CO_2 atmosphere.

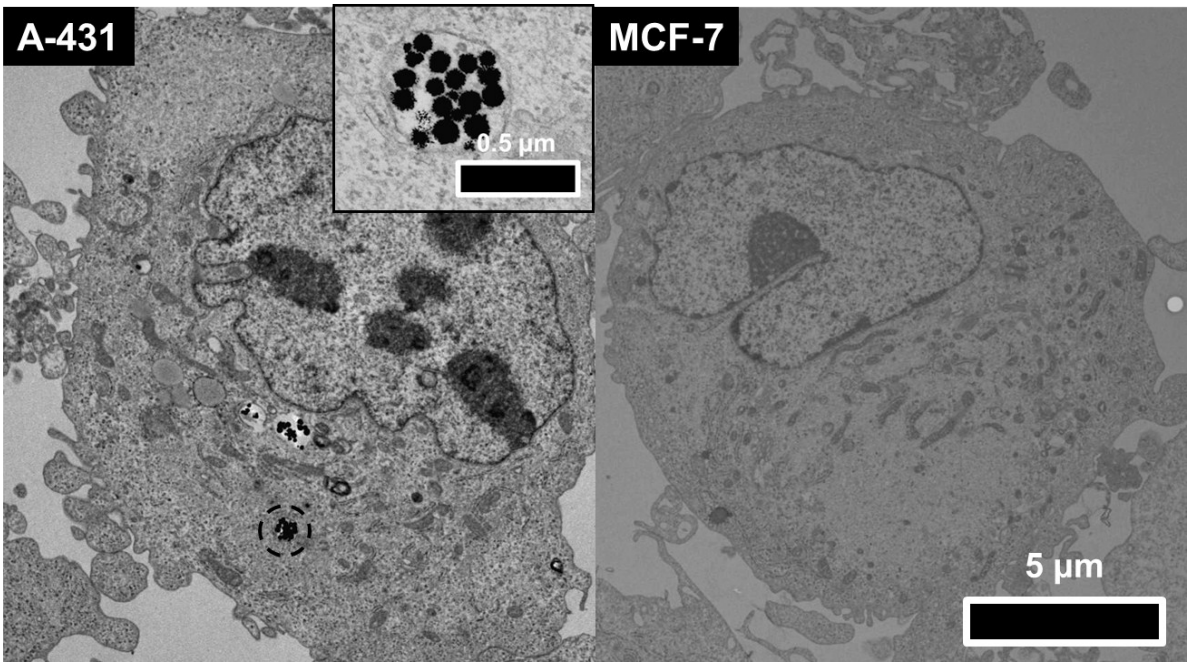

Figure S10. TEM image of A-431 and MCF-7 cells incubated with CG-MPGNs (inset, magnification of the CG-MPGNs in the cytopolasm). CG-MPGNs were internalized via receptor meditated endocytosis (appeared as black dots)

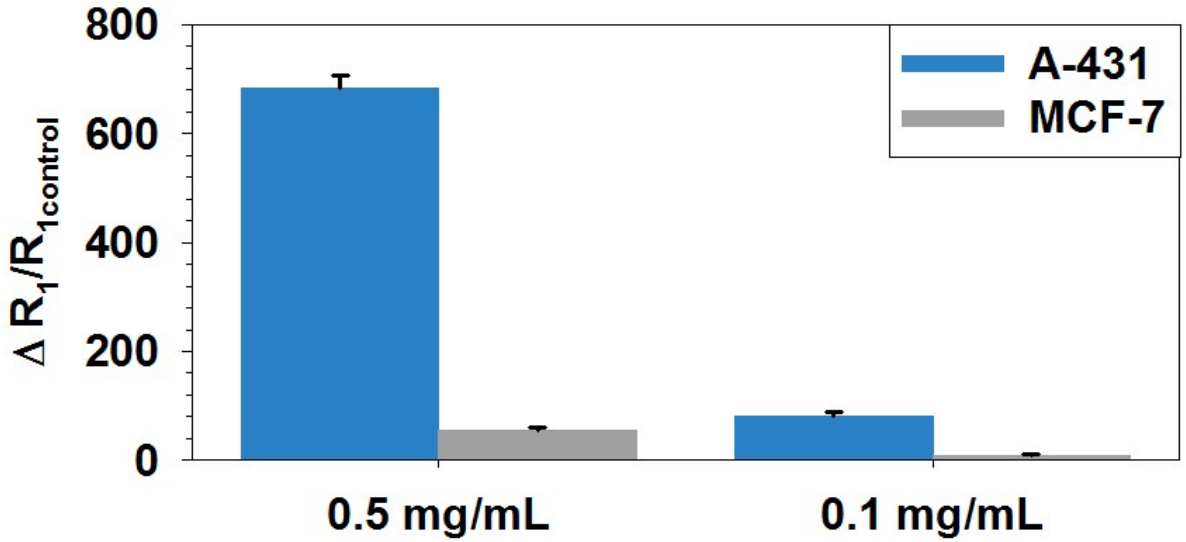

Figure S11. $\Delta R_1/R_{1control}$ graph of A-431 (EGFR+) and MCF-7 (EGFR-) cell lines (1x 10^7 cells each) after treatment with different amounts of CG-MPGNs (0.5 mg/mL and 0.1 mg/mL, respectively) ($\Delta R_1 = R_1 - R_{1ctrl}$). Blue bar graphs represent CG-MPGN-treated A-431 cells. Gray bar graphs represent CG-MPGN-treated MCF-7 cells.

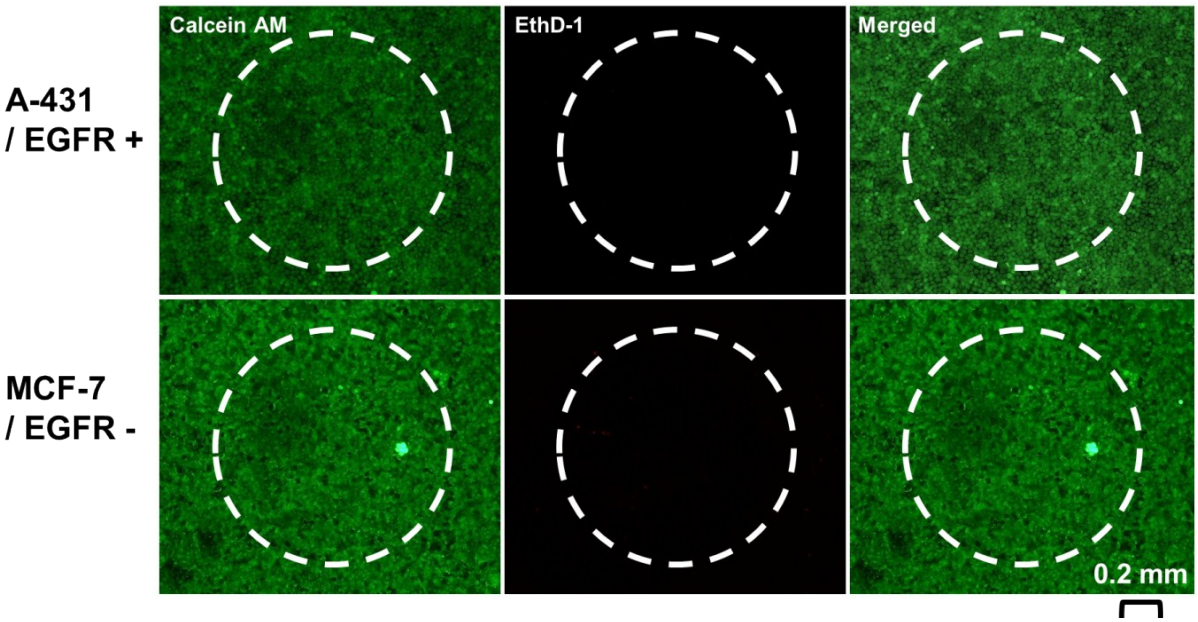

Figure S12. Fluorescence microscopy images of A-431 (EGFR+) and MCF-7 (EGFR−) cells stained with calcein AM and ethidium homodimer-1 (EthD-1) after NIR laser irradiation for 10 min (808 nm, 25 W cm^{-2}). White-dotted curves represent the location of the laser beam. The scale bar represents 200 μm.